Anomalous Stress Response of Ultrahard WB_{n} Compounds

Quan Li, Dan Zhou, Weitao Zheng, Yanming Ma, and Changfeng Chen

Phys. Rev. Lett. **115**, 185502 — Published 29 October 2015

DOI: 10.1103/PhysRevLett.115.185502

Anomalous Stress Response of Ultrahard WB_n Compounds

Quan Li,[1,2,*] Dan Zhou,[3,2] Weitao Zheng,[1] Yanming Ma,[1,†] and Changfeng Chen[2,‡]

[1] *College of Materials Science and Engineering and State Key Laboratory of Superhard Materials, Jilin University, Changchun 130012, China*

[2] *Department of Physics and High Pressure Science and Engineering Center, University of Nevada, Las Vegas, Nevada 89154, USA*

[3] *Laboratory of Clean Energy Technology, Changchun University of Science and Technology, Changchun 130022, China*

(Dated: October 7, 2015)

Boron-rich tungsten borides are premier prototypes of a new class of ultrahard compounds. Here we show by first-principles calculations that their stress-strain relations display surprisingly diverse and anomalous behavior under a variety of loading conditions. Most remarkable is the dramatically changing bonding configurations and deformation modes with rising boron concentration in WB_n (n=2, 3, 4), resulting in significantly different stress responses and unexpected indentation strength variations. This novel phenomenon stems from the peculiar structural arrangements in tungsten borides driven by boron's ability to form unusually versatile bonding states. Our results elucidate the intriguing deformation mechanisms that define a distinct type of ultrahard materials. These new insights underscore the need to explore unconventional structure-property relations in a broad range of transition-metal light-element compounds.

PACS numbers: 62.20.-x,81.40.Jj,61.50.Ah,71.20.Be

Strong covalent solids, such as diamond and cubic boron nitride, contain rigid bonding networks that can sustain large stresses under diverse loading conditions. However, low thermal stability of diamond and high synthesis cost of traditional superhard materials have prompted intensive search for alternative materials that exhibit excellent stability and strength but are easier to synthesize. Recently a new design strategy introduces covalent-bond-forming light elements (LEs) to combine with heavy $4d$ or $5d$ transition metals (TMs) [1–11]. The key idea here is that such TM-LE compounds may benefit from the excellent properties of the constituent components where the heavy TM atoms introduce a high density of valence electrons into the compounds to resist compression while the LE atoms help form a strong covalent bonding network to enhance structural integrity. A high concentration of LE atoms is considered essential to achieving optimal high strength and hardness [7–13].

Outstanding among TM-LE compounds is a series of binary tungsten borides with the LE-to-TM ratio up to 4:1 obtained under relatively easy synthesis conditions [7–9]. These tungsten borides exhibit excellent mechanical properties, making them premier prototypes among this new class of ultrahard materials. Understanding these materials requires a full resolution of their crystal structures complicated by boron's ability to form versatile bonding states [14–17]. We recently identified the structures of WB_n compounds over a wide range of boron content using a global structural search method CALYPSO [18, 19] that has proven effective in solving complex crystal structures [20–23]. The detailed knowledge of the structural arrangements in tungsten borides [24] makes it possible to explore the structure-strength relations and unveil the underlying atomistic deformation mechanisms in these promising materials.

In this work, we determine the stress-strain relations from first-principles calculations for boron-rich tungsten borides WB_n (n=2, 3, 4) under compressive, tensile, pure shear, and Vickers indentation shear strains. Of particular interest is their variation with changing boron content. A positive correlation between strength and boron content has been widely expected, driving extensive recent efforts on the synthesis and characterization of high-boron-content WB_n (n≥3). Surprisingly, our results show no such correlation; instead, we find that the WB_n compounds exhibit versatile stress response at different boron content, and WB_2 shows the best overall strength performance under various loading conditions. This anomalous phenomenon stems from the peculiar bonding arrangements in the WB_n compounds with the changing boron concentration n, which introduces different deformation mechanisms that produce distinct mechanical properties in these boron-rich tungsten borides. Our findings challenge the conventional wisdom and offer key insights into the fundamental structural deformation modes and strength of tungsten borides. These results suggest that unconventional structure-property relations may also exist in a broad range of TM-LE compounds such as other TM borides and TM nitrides and carbides that possess complex bonding configurations.

Tungsten borides adopt a rich variety of structural forms. Our global structure search [24] over a wide concentration range identified five stable tungsten borides; but the two compounds with lower boron concentrations, W_2B and WB, exhibit much lower strength due to a lack of direct boron-boron bonding network, which sets them apart from the three boron-rich WB_n (n=2, 3, 4), and are not regarded as ultrahard and thus not considered in the present work. The experimentally synthesized WB_2 and WB_3 have been assigned the structures with

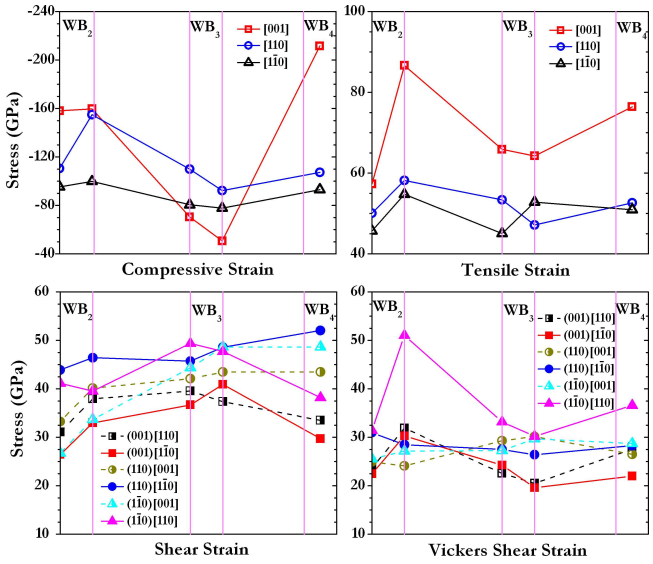

FIG. 1: (Color online) Calculated peak stress values under compressive, tensile, pure shear, and Vickers shear strains for (left to right) $P6_3/mmc$-4u WB_2, $P6_3/mmc$-2u WB_2, $P6_3/mmc$-4u WB_3, R-3m-6u WB_3, and $P6_3/mmc$-2u WB_4.

$P6_3/mmc$-4u and $P6_3/mmc$-4u symmetry, respectively; interestingly, both are metastable according to the calculated convex hull [24]. Calculations also identify thermodynamically stable $P6_3/mmc$-2u WB_2, R-3m-6u WB_3, and $P6_3/mmc$-2u WB_4. We examine these five tungsten boride structures and determine their stress response under various loading conditions. The objective here is to establish fundamental structure-property relations, especially the influence of boron content on mechanical strength and the underlying deformation mechanisms. The results may provide key benchmarks for understanding this new class of ultrahard materials. This is especially important considering boron-rich tungsten boride specimens usually contain multiple phases embedded in an amorphous boron matrix [8], which has impeded efforts to extract clear trends of mechanical properties of each individual phase.

Calculations were carried out using the density functional theory with the Perdew-Burke-Ernzerhof generalized gradient approximation (GGA) [25] for the exchange-correlation energy and a plane-wave basis set as implemented in the VASP code [26]. The electron-ion interaction was described by the projector augmented wave (PAW) method [27] with the $5d^46s^2$ and $2s^22p^1$ as valence electrons for W and B atoms, respectively. The total energy of the structure was minimized by relaxing the structural parameters using a conjugate gradient optimization method [28, 29]. The total-energy and stress calculations used an energy cutoff of 700 eV and Monkhorst-Pack [30] k-point grids of 13×13×5, 15×15×7, 9×9×9, 7×7×5, and 13×13×5 for $P6_3/mmc$-4u WB_2, $P6_3/mmc$-2u WB_2, $P6_3/mmc$-4u WB_3, R-3m-6u WB_3, and $P6_3/mmc$-2u WB_4 structures, respectively. The energy convergence is about 1 meV per atom, with residual stresses and forces in the fully relaxed structures less than 0.1 GPa and 0.001 eV/Å, respectively. The stress-strain relation is obtained by calculating stress response to structural deformation along specific loading paths using a quasistatic relaxation method that simulate various loading conditions and determine the corresponding ideal strength and deformation modes [31–34].

We have determined stress responses along different deformation paths under various types of strains, and the lowest peak stress in each case defines the corresponding ideal strength, which is the minimum stress needed to plastically deform a perfect crystal under that type of strain. These results establish key benchmarks for the intrinsic mechanical property of a material [35–40]. Meanwhile, the stress responses along the paths with higher stress peaks provide additional insights into material behavior under different deformation modes (e.g., along another tensile direction or shear slip plane), and such information is crucial to understanding and optimizing material performance. In particular, to determine the indentation strengths we have carried out stress-strain calculations under indentation shear strains in the low-index crystalline planes where crystal cleavage commonly occur, and the obtained results can be compared to actual indentation measurements that are performed on such cleavage planes.

We have computed full stress-strain curves and determined the peak stress and strain values under various strain conditions [41]. We present in Fig. 1 the calculated peak stresses that offer a comprehensive quantitative description of the value, range and trend of the stress response of WB_n with the changing boron content under each type of strain. Most conspicuous and surprising among these results is a total lack of correlation between the peak stress values and the boron content, which is in stark contrast to the common expectation that the strength of tungsten borides would increase with rising boron content [7–13]. In fact, the stress peaks largely decrease going from WB_2 to WB_3 and then recover, only partially in most cases, for WB_4, making the relatively low-boron-content WB_2 the strongest among them with the best overall strength performance.

The distinct stress responses of WB_n are sensitive to the type of strains applied. Under compressive strains, the stress peaks drop significantly from WB_2 to WB_3 and then largely recover for WB_4 with the highest peak achieved along its [001] direction. Under tensile strains, the peak values initially trend downward or remain essentially unchanged as the boron content rises, and then partially recover. Under pure shear strains, all the stress peaks trend upward from WB_2 to WB_3, but then they move in diverging directions for WB_4, with the lowest peak (i.e., the ideal shear strength) reduced essentially to the same value as that for WB_2. Of particular interest are

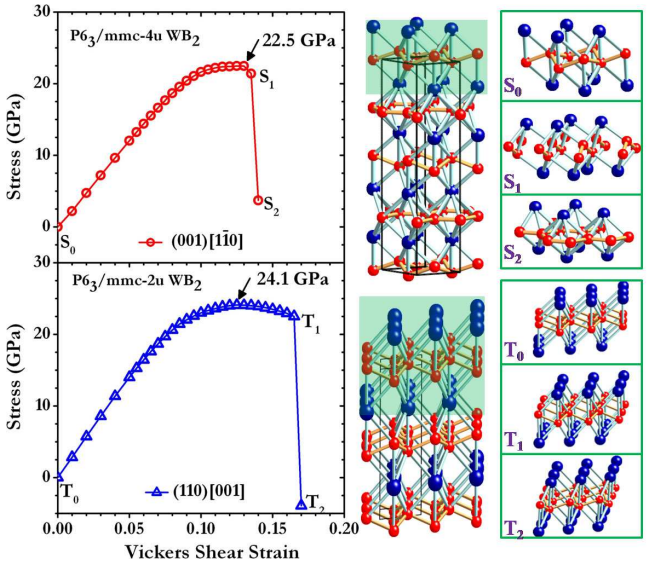

FIG. 2: (Color online) The calculated stress-strain relations and key structural snapshots for the two WB_2 phases in the weakest Vickers shear directions. The small (red) and large (blue) balls represent B and W atoms, respectively, which is also the case in the following figures.

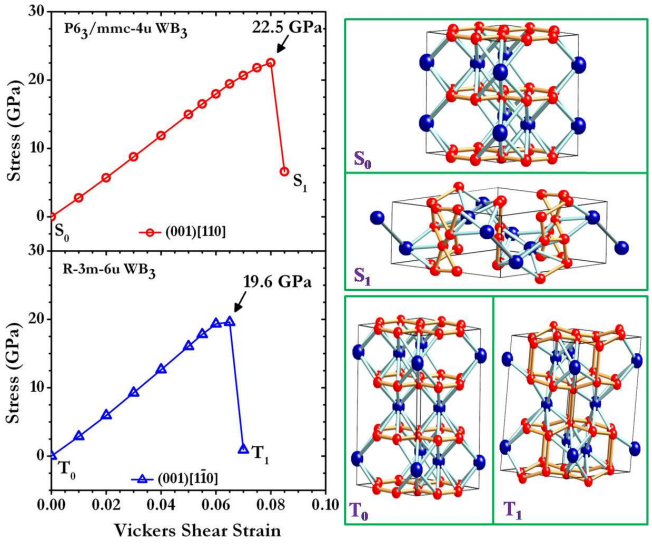

FIG. 3: (Color online)The calculated stress-strain relations and key structural snapshots for the two WB_3 phase in the weakest Vickers shear directions.

the stress responses under indentation shear strains since indentation strength has been the primary focus of recent extensive studies of tungsten borides and other LE-TM compounds. Results in Fig. 1(d) show that the indentation stress peaks trend lower from WB_2 to WB_3 and then rise only slightly for WB_4, but still remain at or below the values for WB_2. Below we analyze the atomistic deformation modes in these WB_n compounds with the lowest stress peaks (i.e., the ideal strength) under indentation strains, and the results also shed light on the anomalous stress variations under other strain conditions.

We first examine the deformation modes in $P6_3/mmc$-$4u$ WB_2 under the indentation strain in the (001)[1$\bar{1}$0] shear direction where the lowest stress peak (i.e., the ideal indentation strength) is obtained (Fig. 2). Structural snapshots show that the slightly buckled boron honeycomb sheet (see the highlighted region in Fig. 2) is the main load-bearing component. Near the peak stress at the indentation shear strain ϵ=0.135, several boron bonds break, turning the boron sheet into zigzag chains. The normal compressive pressure beneath the indentor in the [001] direction squeezes these zigzag chains, resulting in B-B rebonding that leads to the formation of a graphitelike flat honeycomb boron layer, accompanied by a stress release. The situation in $P6_3/mmc$-$2u$ WB_2 is similar, but it involves a different mechanism; instead of a bond breaking and rebonding process, the indentation strains cause a stress concentration that drives a collective bond flipping in the buckled boron sheet (see Fig. 2) to release the stress past the peak value. In general, the boron sublattices in these WB_2 structures form a strongly bonded framework that withstand large deformation strains, while the tungsten atoms provide a high electronic density to resist uniform compression. This is the essence of new design principle for ultrahard TM-LE compounds [1–11]. The strong covalent boron network in WB_2 can produce very high indentation strength in certain crystal orientations; for example, the peak stress under the (1$\bar{1}$0)[110] indentation shear strains reaches 51.0 GPa for $P6_3/mmc$-$2u$ WB_2, which is close to the value for cubic boron nitride. This offers a promising avenue for enhancing the indentation strength through optimal design of crystal orientation relative to the direction of external loading.

We now turn to the two WB_3 phases (Fig. 3), both of which contain large voids in their structures [24]. This structural feature makes them less resistent to compression, thus explaining the large reduction in their peak stresses under compressive strains. This mechanism also underlies the reduction in the indentation strength in WB_3 phases since indentation produces a large compressive strain beneath the indenter, which crushes the boron layers in $P6_3/mmc$-$4u$ WB_3 and significantly reduces the distance between the boron layers in R-$3m$-$6u$ WB_3. Moreover, the resulting large lateral volume expansion perpendicular to the [001] direction induced by the compressive pressure breaks up the honeycomb sheet at a low indentation shear strain ($\epsilon < 0.085$). On the other hand, the strong boron networks in both $P6_3/mmc$-$4u$ WB_3 and R-$3m$-$6u$ WB_3 produce large pure shear strength (36.7 and 37.3 GPa), which suggests that they can resist large deformation in scratch hardness tests where no substantial normal compression is present, making them suitable for applications in hard wear-resistant coatings.

Most intriguing among the tungsten borides is WB_4.

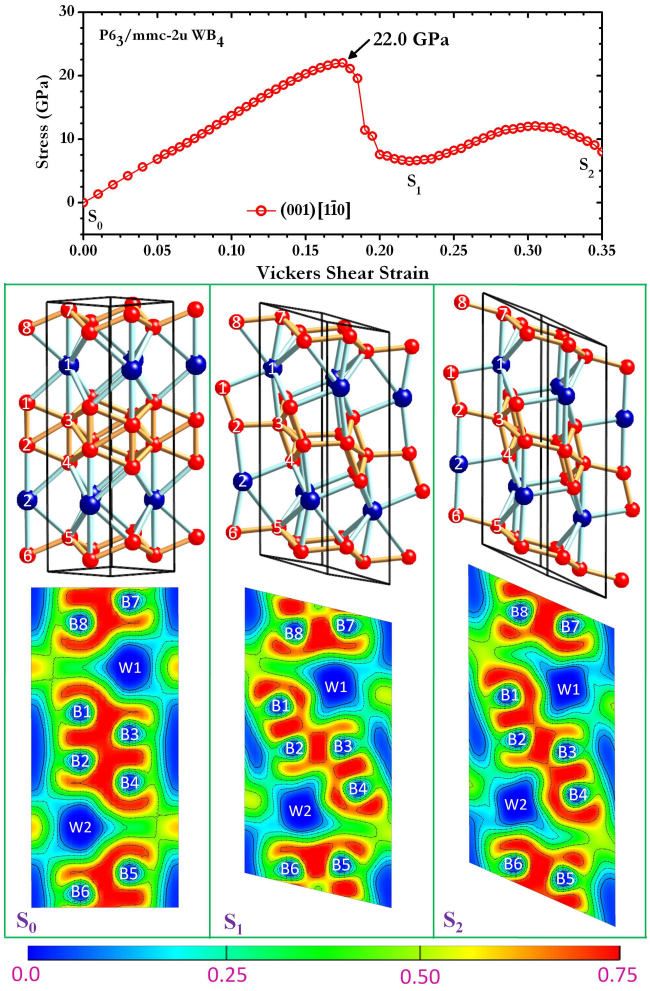

FIG. 4: (Color online) The calculated stress-strain relations and key structural snapshots for the WB_4 phase in the weakest Vickers shear directions. Also shown are the two-dimensional ELF plot in the (1$\bar{1}$0) crystalline plane.

It possesses the highest boron content in a dense bonding network, raising the expectation on superior strength and hardness. Surprisingly, our calculations (Fig. 1d) reveal that the lowest stress peak (i.e., ideal strength) under indentation strains for WB_4 is even slightly lower than the corresponding value for WB_2; moreover, the other stress peaks of WB_4 are not much higher either. Equally striking is the observation that the stress-strain curve (Fig. 4) exhibits a creep-like behavior typically seen in metals but almost never in strong covalent solids. These results point to highly unusual bonding characters in WB_4. Structural snapshots at several key strains (Fig. 4) show that the boron bilayer in the middle of the cell is the main load-bearing component where significant B-B bond stretch and bond breaking occur under large strains. To examine the nature of these bonding states, we plot the electron localization function (ELF) isosurfaces for $P6_3/mmc$-2u WB_4. Three-center bonding is clearly visible in the buckled boron bilayers at equilibrium (Fig. 4), which is made possible by the similar bond lengths of triangular B_1-B_2 (1.725 Å), B_1-B_3 (1.851 Å), and B_2-B_3 (1.982 Å) bonds in $P6_3/mmc$-2u WB_4. As the indentation shear deformation in the (001)[1$\bar{1}$0] direction increases, the B_1-B_3 and B_2-B_4 bonds are continuously stretched, making a smooth transition from the three- to two-center covalent bonding states accompanied by a continuous charge transfer between the three- and two-center bonds. This peculiar transition produces a creep-like stress response with much reduced energy cost, resulting in the low peak stress, without the usual hard bond breaking seen in strong covalent solids such as diamond, cubic BN and BC_2N [32–34, 37, 39] or even lower-boron-content tungsten borides, whose bonding environments do not support the three-center bonds. The multi-center bonding transition in WB_4 considerably constraints its indentation strength, and the same mechanism underlies its low ideal strength under pure shear strains (Fig. 1c). Meanwhile, the smooth transitions between different bonding states produce a simultaneously high-strength and high-ductility state in WB_4, making it suitable for applications where both qualities are desired.

The anomalous stress responses of WB_n have important implications for understanding such a different type of ultrahard materials and guiding their optimization in synthesis and application. In particular, our results suggest that recent efforts almost exclusively focused on high-boron-content WB_3 and WB_4 may be misguided, and that emphasis should shift to the WB_2 phases that, according to our calculations, exhibit the best overall strength performance under various loading conditions.

In summary, our first-principles calculations reveal that, contrary to common expectations, increasing boron content does not lead to higher mechanical strength in boron-rich tungsten borides; instead, their ideal strength values show little improvement or even trend downward with rising boron content in most cases. This intriguing behavior is fundamentally rooted in boron's ability to form versatile bonding states, which produces distinct structural configurations, including the alternating boron and tungsten single-layer arrangement in WB_2, the large voids in WB_3, and the three-center bonds in the boron bilayers in WB_4. While WB_3 exhibits reduced strength due to the conventional structural weakness associated with the large voids, the strength of WB_4 is limited by a more subtle quantum effect, which introduces three-center boron bonds that can transform to two-center bonds via a continuous charge transfer under shear strains. These constraints make WB_2 the best overall choice for high-strength performance; meanwhile, WB_4 shows remarkable simultaneous high strength and enhanced ductility under shear strains. This work represents a comprehensive study of boron-rich tungsten borides based on a global structure search and the results have important implications for a large class of transition-metal borides that share the same boron con-

centration range and likely similar bonding configurations and deformation mechanisms as revealed in the present study. The diverse atomistic mechanisms underlying the striking stress-strain relations in WB_n introduce new knowledge about structural deformation in strong solids, which calls for further studies of a broad range of additional TM-LE compounds to explore their structure-property relations that may also exhibit rich and unexpected phenomena.

This work was supported in part by DOE under Cooperative Agreement DE-NA0001982 at UNLV and NSFC (Nos. 11474125, 51202084, and 11274136) at JLU.

* Electronic address: liquan777@jlu.edu.cn
† Electronic address: mym@jlu.edu.cn
‡ Electronic address: chen@physics.unlv.edu

[1] J. C. Crowhurst, A. F. Goncharov, B. Sadigh, C. L. Evans, P. G. Morrall, J. L. Ferreira, and A. J. Nelson, Science **311**, 1275 (2006).
[2] E. Gregoryanz, C. Sanloup, M. Somayazulu, J. Badro, G. Fiquet, H. Mao, and R. J. Hemley, Nat. Mater. **3**, 294 (2004).
[3] A. F. Young, C. Sanloup, E. Gregoryanz, S. Scandolo, R. J. Hemley, and H. Mao, Phys. Rev. Lett. **96**, 155501 (2006).
[4] S. H. Tolbert, R. W. Cumberland, S. M. Clark, J. J. Gilman, M. B. Weinberger, and R. B. Kaner, J. Am. Chem. Soc. **127**, 7264 (2005).
[5] H. Y. Chung, M. B. Weinberger, J. B. Levine, A. Kavner, J. M. Yang, S. H. Tolbert, and R. B. Kaner, Science **316**, 436 (2007).
[6] J. Q. Qin, D. W. He, J. H. Wang, L. M. Fang, L. Lei, Y. J. Li, J. Hu, Z. L. Kou, and Y. Bi, Adv. Mater. **20**, 4780 (2008).
[7] R. Mohammadi, A. T. Lech, M. Xie, B. E. Weaver, M. T. Yeung, S. H. Tolbert, and R. B. Kaner, Proc. Natl. Acad. Sci. U.S.A. **108**, 10958 (2011).
[8] M. Xie, R. Mohammadi, Z. Mao, M. M. Armentrout, A. Kavner, R. B. Kaner, and S. H. Tolbert, Phys. Rev. B **85**, 064118 (2012).
[9] Q. Gu, F. Krauss, and W. Steurer, Adv. Mater. **20**, 3620 (2008).
[10] X. Cheng, W. Zhang, X. Chen, H. Niu, P. Liu, K. Du, G. Liu, D. Li, H. Cheng, H. Ye and Y Li, Appl. Phys. Lett. **103**, 171903 (2013).
[11] M. Wang, Y. Li, T. Cui, Y. Ma, and G. Zou, Appl. Phys. Lett. **93**, 101905 (2008).
[12] Q. Tao, D. Zheng, X. Zhao, Y. Chen, Q. Li, Q. Li, C. Wang, T. Cui, Y. Ma, X. Wang, and P. Zhu, Chem. Mater. **26**, 5297 (2014).
[13] M. Xie, R. Mohammadi, C. L. Turner, R. B. Kaner, A. Kavner, and S. H. Tolbert, Phys. Rev. B **90**, 104104 (2014).
[14] H. Tang and S. Ismail-Beigi, Phys. Rev. Lett. **99**, 115501 (2007).
[15] A. R. Oganov and V. L. Solozhenko, J. Superhard Mater. **31**, 285 (2009).
[16] A. R. Oganov, J. Chen, C. Gatti, Y. Ma, Y. Ma, C. W. Glass, Z. Liu, T. Yu, O. O. Kurakevych, and V. L. Solozhenko, Nature **457**, 863 (2009).
[17] W. Zhou, H. Sun, and C. F. Chen, Phys. Rev. Lett. **105**, 215503 (2010).
[18] Y. Wang, J. Lv, L. Zhu, and Y. Ma, Comput. Phys. Commun. **183**, 2063 (2012); the CALYPSO code is free for academic use, see details at http://www.calypso.cn.
[19] Y. Wang, J. Lv and L. Zhu, and Y. Ma, Phys. Rev. B **82**, 094116 (2010).
[20] J. Lv, Y. Wang, L. Zhu, and Y. Ma, Phys. Rev. Lett. **106**, 015503 (2011).
[21] L. Zhu, H. Wang, Y. Wang, J. Lv, Y. Ma, Q. Cui, Y. Ma, and G. Zou, Phys. Rev. Lett. **106**, 145501 (2011).
[22] H. Liu and Y. Ma, Phys. Rev. Lett. **110**, 025903 (2013).
[23] M. Zhang, H. Liu, Q. Li, B. Gao, Y. Wang, H. Li, C. Chen, and Y. Ma, Phys. Rev. Lett. **114**, 015502 (2015).
[24] Q. Li, D. Zhou, W. Zheng, Y. Ma, and C. F. Chen, Phys. Rev. Lett. **110**, 136403 (2013).
[25] J. P. Perdew, K. Burke, and M. Ernzerhof, Phys. Rev. Lett. **77**, 3865 (1996).
[26] G. Kresse, and J. Furthmüller, Phys. Rev. B **54**, 11169 (1996).
[27] G. Kresse, and D. Joubert, Phys. Rev. B **59**, 1758 (1999).
[28] M. P. Teter, M. C. Payne, and D. C. Allan, Phys. Rev. B **40**, 12255 (1989).
[29] D. M. Bylander, L. Kleinman, and S. Lee, Phys Rev. B **42**, 1394 (1990).
[30] H. J. Monkhorst and J. D. Pack, Phys. Rev. B **13**, 5188 (1976).
[31] Y. Zhang, H. Sun and C. F. Chen, Phys. Rev. Lett. **93**, 195504 (2004).
[32] Z. C. Pan, H. Sun, and C. F. Chen, Phys. Rev. Lett. **98**, 135505 (2007).
[33] Z. C. Pan, H. Sun and C. F. Chen, Phys. Rev. B **79**, 104102 (2009).
[34] Z. C. Pan, H. Sun, Y. Zhang, and C. F. Chen, Phys. Rev. Lett. **102**, 055503 (2009).
[35] D. Roundy, C.R. Krenn, M. L. Cohen, and J.W. Morris Jr., Phys. Rev. Lett. **82**, 2713 (1999).
[36] S. Ogata, J. Li, and S. Yip, Science **298**, 807 (2002).
[37] Y. Zhang, H. Sun, and C. F. Chen, Phys. Rev. Lett. **94**, 145505 (2005).
[38] Y. Zhang, H. Sun, and C. F. Chen, Phys. Rev. B **73**, 144115 (2006).
[39] Y. Zhang, H. Sun, and C. F. Chen, Phys. Rev. B **76**, 144101 (2007).
[40] J. Yang, H. Sun, and C. F. Chen, J. Am. Chem. Soc. **130**, 7200 (2008).
[41] See Supplemental Material for all the calculated full stress-strain curves and the detailed information on the peak stress and strain values under the compressive, tensile, pure shear and Vickers indentation shear conditions.